Surface deformations from moderate-sized earthquakes in Mongolia observed by InSAR

Sh. Amarjargal[1], T. Kato[2], and M. Furuya [3]

[1]*GPS Geodesy & Geodynamics Group, Research Center for Astronomy and Geophysics, Ulaanbaatar, 210613, POB788, Mongolia*
[2]*Earthquake Research Institute, The University of Tokyo, 1-1, Yayoi 1, Bunkyo-ku, Tokyo 113-0032, Japan*
[3]*Department of Natural History Sciences, Hokkaido University, N10W8, Kita-ku, Sapporo 060-0810, Japan*

We investigate surface deformations associated with two moderate-sized shallow earthquakes that occurred in the southeastern and northwestern stable regions of Mongolia using analysis of ENVISAT/ASAR and ALOS/PALSAR data, respectively. Differential interferograms generated by standard two-pass interferometric analysing technique depicted an uplift of up to ∼1 cm for tne M_W 5.2 Hatanbulag composite earthquake (20 July 2005, moderate size foreshock in three hours) and a subsidence of up to ∼10 cm for the M_W 5.1 Büsiin Gol earthquake (19 January 2008) in the radar line-of-sight directions, respectively. We inverted the observed deformations for the source parameters of the two earthquakes using elastic dislocation modeling. Our preferred models has a geodetic moments of ∼3.83 $\times 10^{17}$ (M_w5.6) and 5.56×10^{16} Nm (M_w5.1) for the Hatanbulag and Büsiin Gol earthquakes, respectively.
Key words: co-seismic displacement, satellite geodesy, InSAR, Mongol earthquakes

1. Introduction

In the past two decades Interferometric Synthetic Aperture Radar (InSAR) has been shown to be a valuable tool for measuring surface deformations induced by earthquakes with unprecedented spatial resolution in many different places on Earth. It has been successfully applied to observations of co-seismic (e.g., Zebker *et al*., 1994), post-seismic (e.g., Peltzer *et al*., 1998), and inter-seismic strain (e.g., Wright *et al*., 2001) associated with a number of large earthquakes. Moreover, its sensitivity to subtle displacements associated with moderate to small-magnitude shallow earthquakes has been demonstrated for example, at the M5.4 (depth 2.6 km) 1992 Landers aftershock (Feigl *et al.,*1995), the M4.7 (depth 0.7 km), M5.0 (depth 3.5 km), M5.3 (depth 3.2 km) and M5.4 (depth 5.2 km) earthquakes in the Zagros Mountains (Lohman and Simons, 2005), using C-band SAR data (wavelength=5.6 cm) and two shallow (∼1 km) M4.7 and M4.4 earthquakes in Western Australia using L-band (wavelength=23.6 cm) and C-band SAR data, respectively (Dawson *et al.,* 2008).

Here, we apply the InSAR technique to two shallow, moderate-sized earthquakes that occurred in remote areas of Mongolia to verify the InSAR detection capabilities in this kind of seismotectonic environments. Although Mongolia is considered to be a tectonically active region located in the transition zone between N-S convergence to the south in the Tien Shan and a NW-SE extension to the north in the Baikal rift (Baljinnyam *et al*., 1993), it still remains the least studied and poorly understood region in northeast Asia because of the lack of seismic and geodetic observations. Since In-

SAR allows surface deformation measurements over vast areas without requiring any ground instrument deployment, it is likely one of the suitable choice to utilize it in the current socio-economic conditions of Mongolia. From the ESA and JAXA datapool we selected and processed interferometric pairs captured either by ENVISAT, Advanced Synthetic Aperture Radar (ASAR) or ALOS, Phased Array type L-type Synthetic Aperture Radar (PALSAR) over six small to moderate (3.9≤ M≤ 5.6) earthquakes that occurred in the territory of Mongolia. Of these, we failed to detect one due to the complete decorrelation of ASAR scenes in the densely vegetated mountainous area (Büsiin Gol, M_w5.4, 27 April 2005), and three were not detected, probably due to the deep depth, lack of data availability or location uncertainties in the seismic catalog as we encontered in the case of the Hatanbulag event, where NSDC (National Seismological Data Center of Mongolia) cataloged location occurred outside of the InSAR frame.

In the current work, we present an analysis of two earthquakes that were successfully detected by conventional interferometric processing using the available data. The first event occurred in Hatanbulag (composite, M_w5.2, 20 July 2005) in the southeastern Gobi (Fig. 1). The second, Büsiin Gol (M_w5.1, 19 January 2008) event, occurred in the Hövsgöl-Büsiin Gol rift (HBR) system in northwestern Mongolia (Fig.2).

2. Tectonic background
2.1 South East Gobi

Hatanbulag is located in southeastern Gobi region of Mongolia, that has long been considered as historically aseismic and tectonically quiescent. This region and most part of eastern Mongolia are covered by nonmarine basins formed during the late Mesozoic extension. The Mesozoic family of basins extend up to 1.5 million km² from the North China

to the south to the Amurian plain to the northeast. The northeast-trending East Gobi Basin (EGB) is one of these basins and together with the Züünbayan faults of the same trend represent the only two prominent geomorphological features of southeastern Gobi (Fig. 1). Various broad discussions characterize the EGB as an extensional and adjacent area as experienced contraction and extension in late Mesozoic time (Zorin, 1999). Basement rocks of the EGB are generally upper Paleozoic flysch and volcanic arc sequences formed in a remnant ocean basin. The region is well known for abundant mineral resources (Oyu Tolgoi Cu-Au-Mo deposit, Dornogovi Ur deposit, Tavan Tolgoi coking coal deposit, oil fields in Tsagaan els and Züünbayan etc.), however tectonic models are still controversial. Rocks in southeastern Mongolia are considered to be a part of the Central Asian Orogenic Belt or Altaids and record history of the amalgamation of Asia via collision and accretion (Sengör *et al.*, 1993). Therefore, data from this region are considered to have important implications in understanding the complex history of intracontinental deformation in Asia (Graham *et al.*, 2001, Webb *et al.*, 2006). Züünbayan and North Züünbayan faults collectively referred in some literature as Züünbayan Fault Zone (ZBFZ) (Lamb *et al.*, 1999) or East Mongolian Fault Zone (EMFZ) (Yue and Liou, 1999), or East Gobi Fault Zone (EGZF) (Webb and Johnson, 2006) follows the southern edge of the Altaid complex (Sengör *et al.*, 1993) running along the EGB, and defines a structural corridor in this region. Yue and Liou (1999) and Lamb *et al.*, (1999) proposed a kinematic linkage between the EGFZ and the Altyn Tagh fault through the Alxa fault, just south of the Mongolia-China border. Both defines the EGFZ as a left-lateral strike-slip fault but differs in the offset and the timing: ∼400 km offset in Cenozoic and ∼200 km offset mainly in Mesozoic, respectively. Evidence for middle-Cretaceous movement on faults within the EGFZ was identified using seismic reflection data by Johnson (2004). Outcrop data evidenced a sinistral strike-slip motion in the Cenozoic time (Webb and Johnson, 2006).

The 20 July 2005 Hatanbulag (HB) earthquake occurred in the uplifted Hutag Uul cratonal block of Badarch *et al.*, (2002) about 9.5 km southwest of Hatanbulag town, ∼50 km south of the Züünbayan fault and ∼30 km north of the unnamed fault (Fig. 1). The Hutag Uul block and Züünbayan fault separate the EGB to the south from its family basin Erlian in northern China. Two foreshocks preceded the mainshock on the same day at 18:06 and 20:02 UTC, first of which has magnitude of $M_W 5.0$ according to the CMT and NEIC catalogs. In August 2011 one of us had chance to visit the earthquake area. As the local people report this earthquake was one of the strongest event they ever felt in this area. During this event, water of the Jirem well (about 2 km west from the epicenter, depth is about 2 m, Fig. 9), from where local people collect their drinking water was disappeared. Owing to the sparse population, no significant damage except some cracks that occurred in a wall of two buildings in the center of Hatanbulag town were reported. Aftershocks rumble in the following two days. The sound and shake were experienced in the Sulinheer town, about 50 km southeast of Hatanbulag town (Fig. 3). There are records of few small earthquakes ($2 \leq M \leq 4.9$) within this region

since 1964 (NSDC, National Seismological Data Center of Mongolia; Fig. 1). The closest recorded moderate-sized earthquake to the Hatanbulag event are the 1983 M4.4 and 1998 M4.7 earthquakes, which were occured over 40 km to the southeast and north, respectively from the current event (Fig. 1).
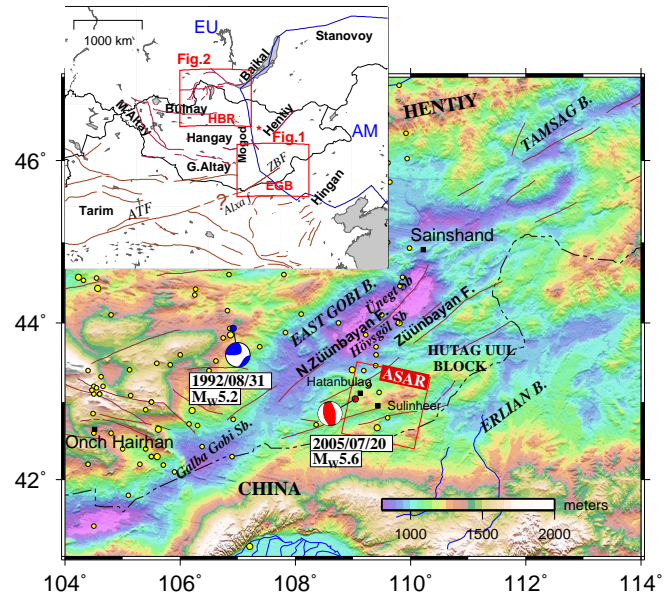

Fig. 1. Topography and major tectonic features of the region surrounding the 2005/07/20 Hatanbulag earthquake. Focal mechanisms are from the Global CMT catalog. Yellow dots show events with magnitudes $2 \leq M \leq 4.9$ that occurred since 1964 (earthquake location data for 1964-2006 from the NSDC Mongolia, 2006-2008 from NEIC). Faults are from the National Atlas of the Mongolian People's Republic. The red boxes in the inset map outline the area represented in Fig. 1 and Fig. 2.

2.2 Hövsgöl-Büsiin Gol graben

In contrast to the eastern part, western and central parts of Mongolia are characterised by high seismic activities and hold main morphotectonic structures of the country. Hövsgöl-Büsiin Gol Rift (HBR) system is the northernmost seismic zone of the country (Fig. 1) that is composed from NS-trending almost parallel sitting to each other three small grabens (120-130 km long and 20-30 km wide) - Büsiin Gol, Darkhad and Hövsgöl, from right to left. These grabens are divided by strongly faulted horst-type mountains and together with the eastern Sayan and EW-trending Tunka graben is accepted to form the southwestern flank of the Baikal rift system (Zonenshain and Savostin, 1981; Baljinnyam *et al.*, 1993). The HBR is truncated in the south by EW-trending Bulnay fault that was ruptured in the sequence of $M_s 8.2$-8.3 left-lateral strike-slip events of 1905. The Bulnay fault together with parallel structures in the Sayan range to the north of the HBR is accepted as caused eastward motion of central Mongolia (Zonenshain and Savostin, 1981).

The HBR area is considered to lie at a junction where the compressional tectonics of western and central Mongolia meet the extensional deformation of the Baikal rift (Delouis *et al.*, 2002; Logachev, 2003; Klyuchevskii *et al.*, 2004). Therefore, locating the boundary between the two contrasting regimes is the object of investigations of many authors. Obtaining an accurate estimate of the focal mechanism and
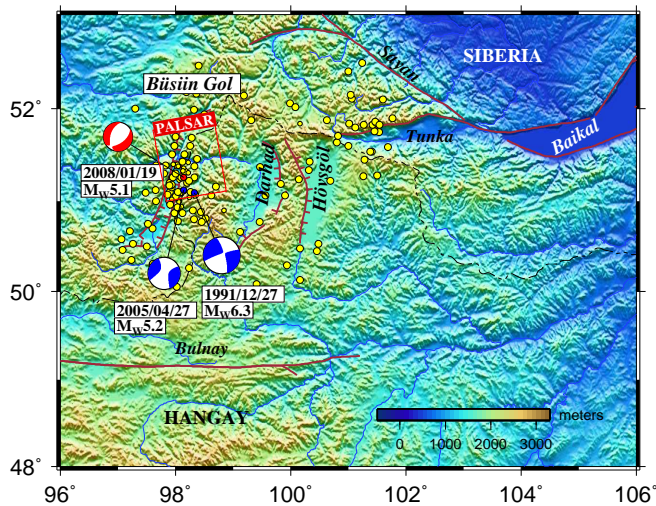
Fig. 2. Topography and major tectonic features of the region surrounding the 2009/01/19 Büsiin Gol earthquake. Focal mechanisms are from the Global CMT solutions: red beachball shows the studied earthquake, blue shows the two recent large events. Only earthquakes with $M \geq 4$ that occurred since 2003 are shown (from NSDC)

.

slip model of the earthquakes is an important for understanding the stress regime of the area as well as for assessing local seismic hazard.

Among three grabens, the asymmetrical Büsiin Gol (BG) is distinguished by a deep, narrow structure and high seismicity. It is about 70 km long and 10-12 km wide. The floor of the graben lies at the 1200 m and is occupied by the wide valley of the Büsiin Gol river and glacial deposits, covered by an impassable taiga, while the mountains of its eastern edge rise up to 3200 m and have inaccessible alp-like peaks (Uflyand *et al.*, 1969). The edges of both sides of the graben are contoured by normal faults, which are considered as formed in the Devonian and Cambrian ages (Uflyand *et al.*, 1969).

About 7000 small and moderate events have been recorded there since 1964 (NSDC). The major events are $M_w 5.5$ (1 April 1976), $M_w 6.5$ (27 December 1991) and $M_w 5.4$ (27 April 2005). The focal mechanism solution of earthquakes in the BG area is a mixture of strike-slip (Delouis *et al.*, 2002; Fig. 2) and normal faulting with predominant strike-slip predominant focal mechanism solution of most earthquakes in the BG area is strike-slip faulting (Delouis *et al.*, 2002; Fig. 2). The 19 January 2008 Büsiin Gol (BG) earthquake discussed in this paper, occurred at the sharp eastern edge of the BG graben.

3. InSAR observations and Results
3.1 Data and Analysis

The co-seismic deformation field of the Hatanbulag earthquake was observed using ASAR C-band data acquired from the descending tracks. From total twelve scenes observed from 13 January 2004 to 02 January 2007 in different seasons, seven belongs to the pre-event and five to the post-event times.

The investigation of the Büsiin Gol event was undertaken using eight PALSAR L-band data acquired from the ascending tracks between 04 January 2007 and 08 April 2008. The

PALSAR data set comprises both Fine Beam Single (FBS) and Fine Beam Dual (FBD) mode data mostly of the winter season. Two from the total of eight scenes belongs to the post-event time. Scene coverage for each radar is shown in the location maps of Fig. 1 and Fig. 2. Each scene of ASAR and PALSAR data covers 100×100 km and 70×70 km area, respectively. Both datasets well suite for applying to the landscapes of the corresponding study sites: C-band data to the dry, sparse vegetated Hatanbulag area with gently undulated terrain, and longer wavelength L-band data to the densely vegetated and highly rugged terrain of the Büsiin Gol area. Except for the deeper penetration capability to the dense vegetated area, L-band data has the longer critical baseline of 13.1 km in Fine Beam Single (FBS) mode and 6.5 km in Fine Beam Dual (FBD) mode compared to 1.1 km of C-band ASAR data. The major disadvantage of L-band data is that the ionospheric effects are expected to be more than twenty times stronger than in C-band. Also, due to the long wavelength, the sensitivity of the PALSAR to small deformations is limited, and interpretation of single interferograms is complicated by the presence of atmospheric and topographic noise. In contrast to the ionosphere, the highly variable lower atmosphere has a similar effect on both frequencies and this remains a major limiting factor for any InSAR observations. Since both ASAR and PALSAR data sets have small off-nadir angles (23 and 38.7 degrees at the center of the scenes, respectively) they are mostly sensitive to vertical displacements.   We processed the data

Table 1. ASAR and PALSAR Interferogram characteristics.

inf	Date1	Date2	$B_{\perp}$, (m)	B_{temp}, (days)	h_a, (m)
ASAR (20 July 2005, Hatanbulag)					
hinf1	2005/02/01	2006/02/21	-57	385	-152
hinf2	2004/01/13	2007/01/02	93	1084	92
hinf3	2005/02/01	2005/03/08	344	37	25
PALSAR (19 January 2008, Büsiin Gol)					
binf1	2007/10/07	2008/02/22	1554	138	33
binf2	2008/01/07	2008/02/22	877	46	59
binf3	2007/10/07	2008/04/08	2120	184	24
binf4	2008/01/07	2008/04/08	1443	92	35.7

from raw format following standard procedures of two-pass approach (Massonet and Feigl, 1998) using the GAMMA software (Wegmüller and Werner, 1997). All images were aligned to one selected reference image, which allows construction of any interferometric combination. The coregistration of images was performed with sub-pixel accuracy. To enhance the signal-to-noise ratio (SNR), the ASAR interferograms were down-sampled by a factor of ten and two in the azimuth and range directions, respectively, resulting in 40 m × 40 m ground pixel. The PALSAR interferograms were down-sampled by a factor of nine in azimuth and three in range directions, resulting in 28 m × 28 m ground pixel. In addition, we applied an adaptive power spectrum filter (Goldstein and Werner, 1998) to suppress the spatial noise in the interferograms. The removal of the topographic phase and the transformation from radar to geographic coordinates were carried out using a 3 arcsec digital elevation model

(DEM) produced by the NASA Shuttle Radar Topography Mission (SRTM) (Farr *et al.*, 2007). The ENVISAT satellite position was modelled using the precise orbit data (Scharroo and Visser, 1998) provided by the DEOS (Delft Institute for Earth-Oriented Space Research), while the ALOS satellite position was modelled with the precise orbit data supplied with the PALSAR metadata. Any residual orbital errors were further minimized through removal of the planar trend surface from each interferogram. The baseline refinement was performed using the unwrapped phase and the same DEM. The phase unwrapping was undertaken using the Minimum Cost Flow (MCF) algorithm, where low-quality pixels are masked out, the remaining data are triangulated and residues are identified. PALSAR data processing includes an additional step of oversampling of FBD data by a factor of two in the range direction before coregistration in order to transform them to the same pixel spacing as the FBS data.

3.2 InSAR Results

3.2.1 Hatanbulag earthquake

In general, the correlation of ASAR radar images was exceptionally good. Even our longest time spanning interferogram (about 3 years between 2004 and 2007) shows relatively high coherence except small decorrelations in the NE-SW trending Harmagtain Gobi valley to the south of the scene and in the valley to the north of the scene (see Fig. 3). The scenes cover almost flat terrain (100 m height differences) of dry bare ground with sparse vegetation and scatterred small lakes and ponds, specific for desert basins. However, some of our scenes were obviously affected by atmospheric artifacts such as a precipitation, severe wind, or sand and dust storms that usually occur between February and May in this region. This is represented in some pre-seismic interferograms by the appearance of concentric fringes at the Halzan Dovny lake, western margin of the deformation field (Fig. 3), and in dried marshes and lakes of the Harmagtain Gobi valley, and by the significant contamination of the most promising co-seismic pairs in terms of temporal coverage. Our assumption has been approved by the weather report data, provided by the Meteorology, Hydrology and Environment Monitoring Center (MHEMC) of Dornogovi province (N. Enkhmaa, Director of MHEMC, personal communication, 2011). In between and at the date of SAR image acquisitions in the period of February 2004 to September 2006, there were many days with emergency records of severe dust and snow, rain storms with the speed of 14-20 m/s. It is not clear when lakes and marshes have been dried, but by the first visit to the earthquake area in the late August of 2011, we found only a mud is left at the location of the Halzan Dovny lake, which probably is moistured time to time only by precipitation. The concentric fringes in the pre-seismic interferograms can either be a thin layer of snow accumulation or soil swell at that locations, if lakes were already dried at that time.

From all possible combinations of twelve ASAR scenes, we investigated twenty nine interferograms with perpendicular baselines ranging from 2 to 482 m, of which eleven contain pre-seismic, thirteen co-seismic and five post-seismic information. We show in Table 1 only two independent co-seismic interferograms and one pre-seismic interferogram, which were selected for subsequent analysis.

All thirteen co-seismic interferograms, with different time spans and values of h_a (the altitude variation producing a phase change of 2π), reveal domal uplift of the surface with a maximum displacement of up to $\sim$10 mm in the line-of-sight (LOS) direction although many of them were contaminated. Among all co-seismic interferograms, the cleanest were those generated from the pair acquired nearly at the same season or month such as 2005/02/01-2006/02/21 (*hinf1*, Fig. 3), 2005/03/08-2006/02/21 (not shown) and 2004/01/13-2007/01/02 (*hinf2*). The maximum LOS displacement on both *hinf1* and *hinf2* is about $\sim$9 mm. The deformation pattern, in general, is elliptical, with minor and major axis estimated to be approximately $\sim$ 8 and 12 km, respectively, stretching roughly NS. For the sake of space, we present only subset of two cleanest interferograms for the HB (Fig. 4a, 4b) as well as for the BG (Fig. 6a, 6b) earthquakes.
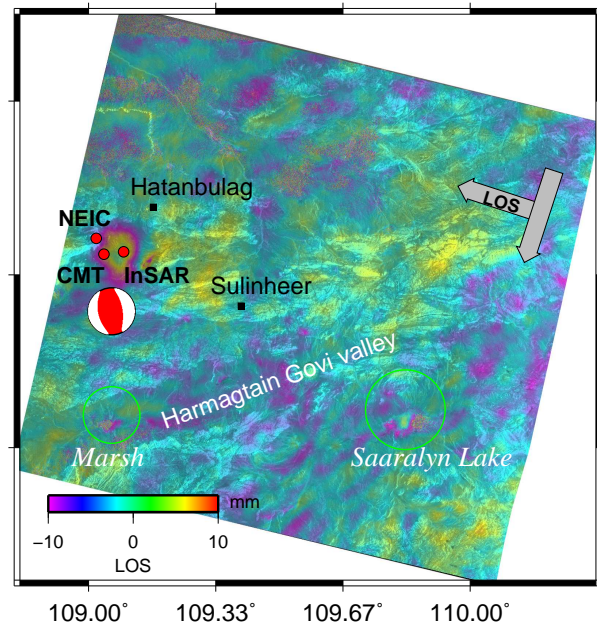

Fig. 3. Geocoded interferogram (scaled to yield displacement in units of mm of range change) spanning 385 days (*hinf6*). Positive LOS displacements are toward the satellite. The LOS direction is shown by the gray arrow. Red dots show seismic locations from the CMT and NEIC catalogs, and the InSAR solution. More westerly NSDC location falls outside of the map frame. The beachball represents the CMT solution.

About 2.6 km to the east of this uplifted pattern, all co-seismic interferograms also reveal a small area of displacements away from the radar, stretching 3 km in NE-SW direction. Although the affected area here is small, the amplitude of the deformation signal is almost the same as for the uplifted area, reaching up to -8 mm. This deformation is observed with almost the same magnitude in three independent interferograms but is not visible in any pre-seismic interferograms. In order to reduce atmospheric noise, residual orbit error and in addition to ensure that the derived signal is actually related to surface deformation, we performed a stack of interferograms. The stacking of independent interferograms improves the ratio of the displacement signal to the atmospheric phase error by a factor of $\sqrt{N}$, where N is number of interferograms (Strozzi *et al.*, 2000). We stacked the co-seismic and pre-seismic interferograms separately having excluded those scenes which have obvious atmospheric ar-

tifacts. The stacking produced cleaner interferograms with a reduced noise levels, but preserved the NE-SW trending small negative signal. Stack of the pre-seismic interferograms did not display any distinct features at the event location, but, as previously noted, it revealed very clear concentric fringes at the small lake Halzan Dovny and Jirem well and in marshes and lakes of the Harmagtain Gobi valley.
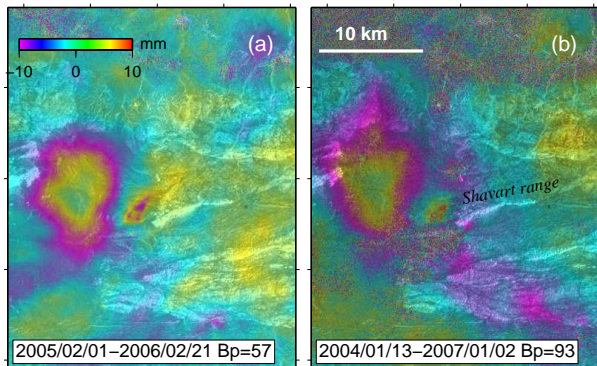

Fig. 4. Subset of observed co-seismic interferograms for the Hatanbulag earthquake: (a) *hinf1* and (b) *hinf2*. $B_\perp$ is the perpendicular baseline in meters.

The negative NE-SW trending signal appears at the same location with the same shape after implementing of three-pass differential interferometry using the "internal" DEM derived from the radar scenes. The shortest time spanning pair 2005/02/01-2005/03/08 with the perpendicular baseline $B_\perp$ = 344 m was used as topographic reference assuming there was no deformation during this period and the 2005/02/01-2006/02/21 pair (*hinf6*) was used as the pair containing the deformation signal. The results of the above test procedures leads to associate this questionable pattern with the surface displacement but not with atmospheric or topographic artifacts. The *height of ambiguities* of our interferograms are between 92 m and 152 m, therefore the error in the SRTM DEM might lead to a phase error of up to $\frac{\sigma_{DEM}}{h_a} = \frac{16m}{152m}$ or about 0.1 cycle. For ASAR acquisitions it corresponds to ~2.8 mm.

3.2.2 Büsiin Gol earthquake

Despite the rugged terrain with differences in elevation of more than 1000 m and dense larch forest cover, the L-band interferograms showed high coherence (see Fig. 6a), allowing successful phase unwrapping for the entire scene in contrast to the interferograms made from the C-Band ASAR data in our attempt on the $M_w5.4$ earthquake (27 April 2005) about 30 km south of the currently studied event (blue beachball in Fig.2), as noted in the Introduction section of this paper. To compare with the Hatanbulag, for the 19 January 2008 Büsiin Gol earthquake we had a limited number of acquisitions, among which there are only two post-seismic data. In addition, most of our interferograms were contaminated by heterogeneous atmospheric propagation, snow cover or layover and foreshortening effects. We were able to construct four co-seismic interferograms using three FBS and one FBD PALSAR images acquired between October 2007 and April 2008. Two interferograms *binf2* and

binf4 have highest percentage of coherent area (100 to 95%) while *binf1* and *binf3* were coherent partly due to the temporal decorrelation. The *binf2* pair has the shortest time span of 46 days and a somewhat small perpendicular baseline of $B_\perp = 877$ m, though the interferogram contains anomalous artifact, which is seen in a broad area extending latitudinally across the scene, to the south of the epicentral location in spite of the planar trend surface removal (Fig. 5). This broad signal might be attributed to the orbital error, or tropospheric and ionospheric variations, however, it did not appear in any other interferograms that share either images that form *binf2* (2008/01/07 and 2008/02/22).
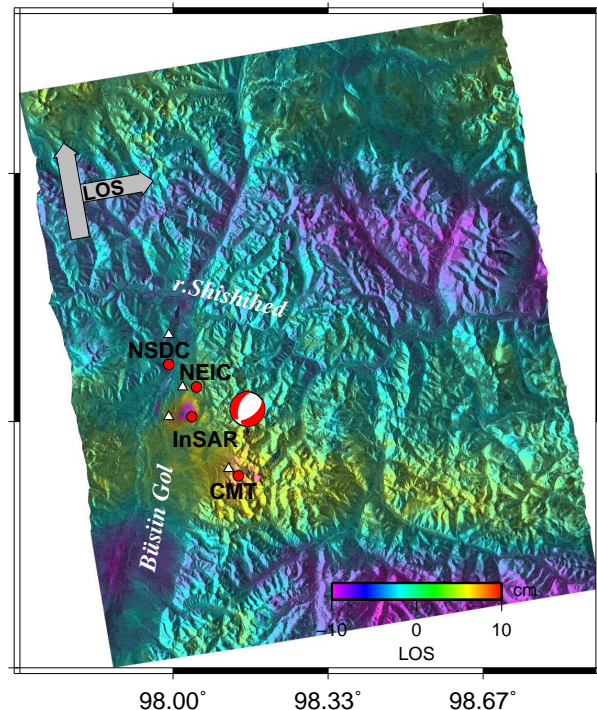

Fig. 5. Geocoded displacement map (unwrapped and scaled to 0.1m/color-cycle) spanning 46 days and generated from pair 2008/01/07-2008/02/22 (*binf2*). White triangles indicate the location of small to moderate shallow eartqhaukes recorded by co-seismic interferograms (see Table 4). Other notations are the same as for Fig. 3

Nevertheless, all of the above discussed interferograms revealed an elliptical deformation pattern with similar dimensions and orientation near the epicenter of the 19 January 2008 earthquake (Fig. 6). The deformation pattern elongates in NE-SW direction and corresponds to ~90 mm negative displacement (ground subsidence) in the LOS direction. The cleanest deformation signal was observed on two interferograms generated from pairs 2008/01/07-2008/02/22 (*binf2*) and 2008/01/07-2008/04/08 (*binf4*, Fig. 6). On these two interferograms major and minor axes of the deformation field reach 6 and 4 km, respectively, and the amplitude of the displacements in the LOS direction was 80 and 110 mm, respectively. However, we have to consider also the topographic errors which are potentially important for this region of high elevation and rugged topography coupled with the relatively long perpendicular baseline of ALOS. If we assume that the SRTM DEM accuracy does not exceed the given theoretical value then the topographic contribution to the measured
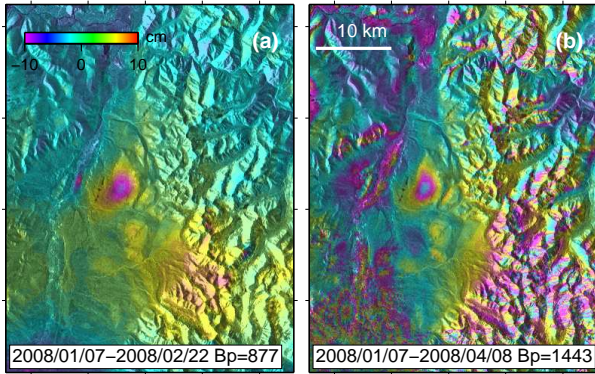
Fig. 6. Subset of observed co-seismic interferograms for the Büsiin Gol earthquake: a) *binf2* and b) *binf4*.

LOS displacement is about 1/4 cycle or 30 mm, calculated from the highest h_a value of the *binf2*, or almost 38% of the observed average LOS displacement of 80 mm.

4. Modeling Results

To explain the observed deformation pattern, we performed both forward and inverse modeling. We represent faults as a rectangular dislocations with either uniform or distributed slip, embedded in a homogeneous, isotropic, elastic half-space (Okada, 1985). We started with a series of forward modeling (Feigl and Dupre, 1999) using the CMT solutions as a priori data, constrained with the observed lobe shape and narrow fringe gradient. We estimated the longitude, latitude, depth z, dip δ, strike α, strike-slip, dip-slip and dimensions of the best-fitting fault plane. In the inverse modeling we optimized the fault geometry and attempted to derive slip distribution using non-negative least-square approach with smoothing constraint on the slip distribution. The inverse solution simultaneously minimizes the L-2 norm of the data misfit and the model roughness:

$$min[\|\mathbf{Gm} - \mathbf{d}\|_2 + \varepsilon^{-2}\|\mathbf{Lm}\|_2], \qquad (1)$$

where the first term $\|\mathbf{Gm} - \mathbf{d}\|_2$ is the L-2 norm of the data misfit and the second term $\varepsilon^{-2}\|\mathbf{Lm}\|_2$ is a measure of the model roughness. $\mathbf{G}$ is the Green's function, that describe how slip on a fault produces displacement at the surface, $\mathbf{d}$ is the observed displacements, $\mathbf{L}$ is the discrete Laplacian operator and $\mathbf{m}$ is a vector of model parameters. Inclusion of Laplacian smoothing in this solution avoids a sharp transition of slip between patches, while non-negativity constraints prevents from changing the sign of the fault patches. For this step, we reduced the volume of the InSAR data to more manageable size by subsampling from 10^6 data points to 10^3. Since the deformation data are highly correlated spatially, it can be reduced without losing significant information. First, we subsampled interferograms by a factor of six along both the range and azimuth directions. Then the subimages were cropped to the region of interest. For the modeling we used the average of two cleanest independent interferograms *hinf1* and *hinf2* for the Hatanbulag earthquake and *binf2* and *binf3* for the Büsiin Gol earthquake. The data were down-sampled using a quadtree partitioning

algorithm (Jónsson *et al.*, 2002) with a threshold value of 2.5 mm for the Hatanbulag interferograms and 2 cm for the Büsiin Gol interferograms because of the small magnitude of the earthquakes. In the quadtree algorithm, the scene is divided into four quadrants and the mean of each quadrant is calculated. If the rms scatter about the mean exceeds a given threshold, the quadrant is subdivided into four new quadrants and the mean is calculated, and compared with the data. The process continues iteratively until convergence. The observed and quadtree decomposed interferograms for both earthquakes are shown in Figures 7 and 8. Based on the obtained best fit fault parameters, we calculated the seismic moment $M_0 = \mu LWU$ (Aki, 1972) and the moment magnitude $M_w = (\log_{10} M_0 - 9.11)/1.5$ (Hanks and Kanamori, 1979) from the fault length L, width W, the displacement U, and by assuming rock rigidity $\mu = 30$ GPa.

4.1 Hatanbulag earthquake

The deformation for the Hatanbulag earthquake was found to cover a large area about 8×12 km^2 but with a peak-to-peak magnitude of only 8-10 mm. This small displacement was revealed despite the likely presence of water bodies (or snow wreath in some lake and marshes after the snow/dust storm) and sand dune drift in the small depression, where the epicenter is located. We obtained solutions for two cases with and without the questionable subsiding pattern to the east. The model that includes the eastern subsidence revealed a strike-slip mechanism with a fault plane size of 1.8×1.3 km^2 at a depth of 6.3 km and 1.3 m of slip. However, the modeled pattern did not match well the observed displacement and the type of faulting is not consistent with the focal mechanism estimated previously from seismograms.
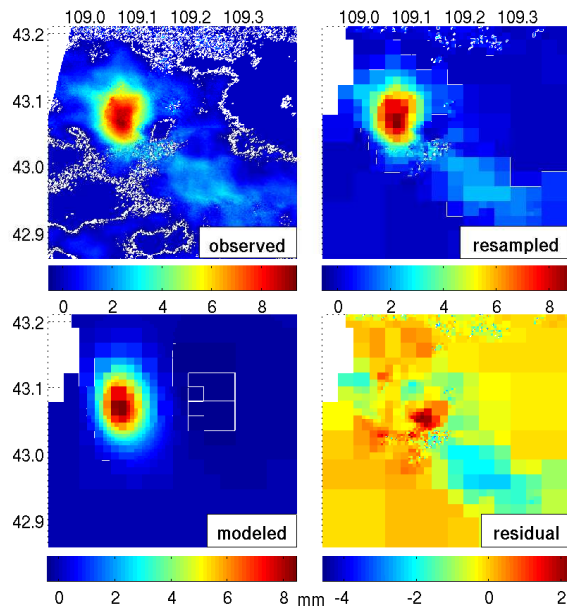

Fig. 7. Inversion results for the Hatanbulag earthquake. The observed (average of two independent interferograms) and resampled data are shown in the top panels, and the modeled and residual interferograms are in the bottom panels with the color bar indicating LOS deformation in mm

The model without the eastern subsidence revealed a thrust type mechanism with a small left-lateral component

and best fits to the observations and the CMT and NEIC fault orientations. The preferred model has a nodal plane that strikes 352°with 0.2 m of strike-slip, dips 49°NW with 0.42 m of dip-slip motion, and has a rake of 64°(Table 3). The best compromise between seismic moment and depth was found for a plane that lies at a depth of 8.3 km with a geodetic moment of $M_0 = 3.83 \times 10^{17}$ Nm ($M_w 5.65$). Observed, modeled and residual interferograms (calculated by subtracting model displacements from observed one) are shown in Fig. 7. The residual interferogram exhibits a major misfit of about 2 mm at the southeastern end of the deformation field, corresponding to the unmodelled subsidence, which we attributed to a local non-tectonic event (Fig. 7). The rms error for this model is 2.3 mm. The position and orientation of the fault plane agree well with the NW-dipping nodal plane of the Global CMT and NEIC solutions. The rake is consistent with the NEIC estimation but differs by 30°from those of the CMT. The geodetic moment is five and four times greater than the seismic moments of the CMT and NEIC solutions, respectively (Table 2).

Table 2. Source parameters of the Hatanbulag earthquake from seismology

Parameters	CMT	NEIC	NSDC
	mainshock at 21:54 UTC		
Longitude (°)	109.04	109.02	108.71
Latitude (°)	43.04	43.07	42.97
Depth [a](km)	12	6	2
Strike (°)	166/352	171/303	-
Dip (°)	41/49	49/53	-
Rake (°)	86/94	127/56	-
M_w	5.2	5.2	$M_L 5.69$
M_0 (N m)	7.36×10^{16}	9.1×10^{16}	-
	foreshock at 18:06 UTC		
Longitude (°)	109.06	109.26	108.98
Latitude (°)	43.01	43.045	43.12
Depth [a](km)	12	17	15
Strike (°)	13/150	-	-
Dip (°)	41/58	-	-
Rake (°)	125/64	-	-
M_w	5.0	5.0	$M_L 3.5$
M_0 (N m)	4.53×10^{16}	-	-

Table 3. Earthquake source parameters of the Hatanbulag earthquake from InSAR estimates. [a]The location and depth refer to the bottom left of the fault rectangle, following the convention of Okada (1985).

Longitude (°)	Latitude (°)	Depth[a] (km)	Strike (°)	Dip (°)	Rake (°)
109.092	43.045	8.3	352	49	64
Length (km)	Width (km)	Slip (mm)	Moment (Nm)	M_w	
5	5.5	465	3.83×10^{17}	5.65	

4.2 Büsiin Gol earthquake

The deformation associated with the Büsiin Gol earthquake covered smaller area of 6×4 km^2 but had a higher peak-to-peak magnitude of 8-10 cm, typical for the shallow depth events. The preferred best fitting fault model is estimated to be about 1.8 km long along strike and extends to a

depth of 2.4 km. It strikes N52°E with 0.3 m of strike-slip and dips 49°NW with 0.57 m of dip-slip motion (Table 5). The InSAR estimated location for this earthquake is in good agreement with all three seismic solutions with the closest proximity to the NEIC estimation (4.4 km difference) while the CMT and NSDC place it in about 11 km southeast and 8 km northwest, respectively. We note that the location uncertainty of the NSDC estimation for this event is relatively low to compare with those for the HB event, presumably, owing to the inclusion of the Russian Altay-Sayan network north to the BG event in the seismic processing (Dugarmaa *et al.*, 2006, Klyuchevskii *et al.*, 2007). The strike, dip and rake estimated based on InSAR data agree within ∼3°with those of the CMT solution. The residual between the observed and modeled data is no more than 1 cm (Fig. 8), that is within the magnitude of the data errors. The rms error for this model is 2.4 cm. The moment is 5.56×10^{16} ($M_w 5.1$), slightly larger than the CMT estimate of 4.91×10^{16} (Table 4).
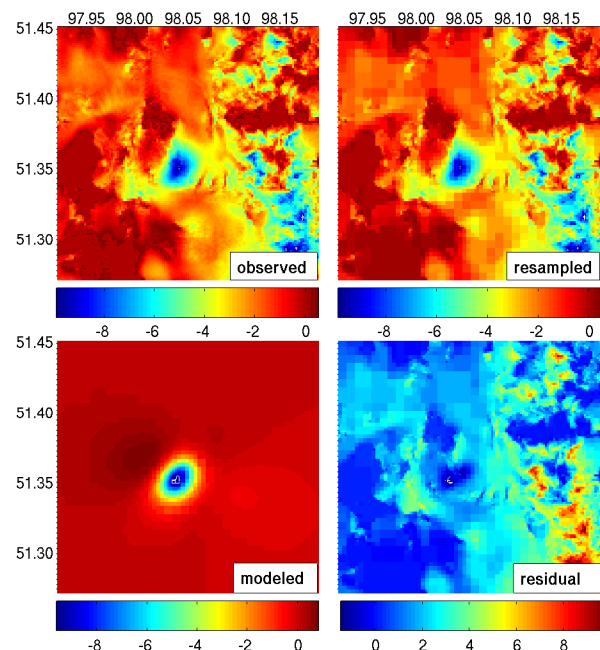

Fig. 8. Inversion results for the Büsiin Gol earthquake. The observed and resampled data are shown in the top panels, and the modeled and residual interferograms are in the bottom panels with the color bar indicating LOS deformation in cm.

Table 4. Earthquake source parameters for the Büsiin Gol earthquake from seismology

Parameters	CMT	NEIC	NSDC
Longitude (°)	98.14	98.05	97.99
Latitude (°)	51.26	51.38	51.41
Depth (km)	12	13	2
Strike(°)	194/56	-	-
Dip (°)	46/52	-	-
Rake (°)	-121/-61	-	-
M_0 (Nm)	4.91×10^{16}	-	-
M_w	5.1	5.1	4.86

Table 5. Earthquake source parameters for the Büssin Gol earthquake from InSAR. [a] The location and depth refer to the bottom left of the fault rectangle, following the convention of Okada (1985).

Longitude (°)	Latitude (°)	Depth[a] (km)	Strike (°)	Dip (°)	Rake (°)
98.04	51.34	2.4	52	49	-62

Length (km)	Width (km)	Slip (mm)	Moment (Nm)	M_w	
1.8	1.6	644	5.56×10^{16}	5.1	

5. Discussion

We compared our InSAR estimates with three seismological solutions (CMT, NEIC and NSDC) although there are some inconsistencies between these catalogs.

Hatanbulag. For this composite event the seismic catalogs show a significant discrepancy. The InSAR-derived moment $M_0 = 3.83 \times 10^{17}$ Nm ($M_w 5.65$) is five and four times greater than the seismic moments of the CMT ($M_0 = 7.36 \times 10^{16}$ Nm) and NEIC ($M_0 = 9.1 \times 10^{16}$ Nm) estimates, but moment magnitude agree well with the NSDC. The strike and dip agree well with the CMT estimate, while the rake and depth agree with the NEIC estimate. In general, discrepancy in moments between InSAR and seismology may be caused by a number of factors including contributions from pre- and post-seismic deformations, or assumptions about the elastic moduli used in the moment estimate. For our study, the HB co-seismic interferograms used for modeling incorporate the moderate magnitude $M_w 5.0$ foreshock according to the CMT (4.53×10^{16}) and NEIC (moment is not reported) and also include the post-seismic deformation since they cover several months and years after the earthquake. However, the contribution of the foreshock may be small, because all three seismological catalogs locate the foreshock below 12 km depth, and the NEIC and NSDC locate the foreshock further away from the mainshock (NEIC in ∼20 km southeast, NSDC in ∼27 km northeast, Table 2). In addition as inferred from the InSAR analysis, the NSDC catalog has a location uncertainty for the mainshock of about 30 km that its location occurred outside of the InSAR frame while the CMT and NEIC estimation agree well within about 4 and 6 km, respectively. Adding the CMT reported moments for the fore- and mainshock yields a total seismic moment of 1.19×10^{17} Nm. This is still lower but three times than the InSAR estimated value.

Similar discrepancies were found for the Zagros earthquakes studied by Lohman and Simons (2005) and Nissen *et al.*, (2010). To adequately constrain these events, it will be neccessary to perform more sophisticated modeling that includes both the seismic and InSAR data. This event is an example demonstrating limitation of the InSAR in distinguishing multiple earthquakes that occurred in the same place or nearby location, which adds an uncertainties in the estimation of both the moment and the focal mechanism.

The observed questionable subsidence pattern presumably related to the local post-seismic process, hydrological effects or topography-correlated atmospheric artifact. The latter assumption is most likely supported based on the examination of the Landsat ETM, relief (from the field visit) and radar amplitude images. The questionable pattern corresponds to the NE-SW trending small topographic high surrounded by dry streambeds, west of the Shavart range (Fig. 9).

Büsiin Gol. The InSAR estimate for this event agrees relatively well with three seismological estimates for all parameters with small uncertainties. The radar estimate of the epicentral location is closest to the NEIC estimated value within 4.4 km, while the CMT catalog has uncertainty of about 11 km. The InSAR determined depth of 2.4 km agrees well with the NSDC estimated depth, while both CMT and NEIC place it deeper to 12 and 13 km, respectively, which is not common for the Büsiin Gol area and may be less reliable for detection it with InSAR. For this event discrepancy in the moment between InSAR-derived 5.56×10^{16}Nm and the 4.91×10^{16}Nm of seismological estimate is relatively small.
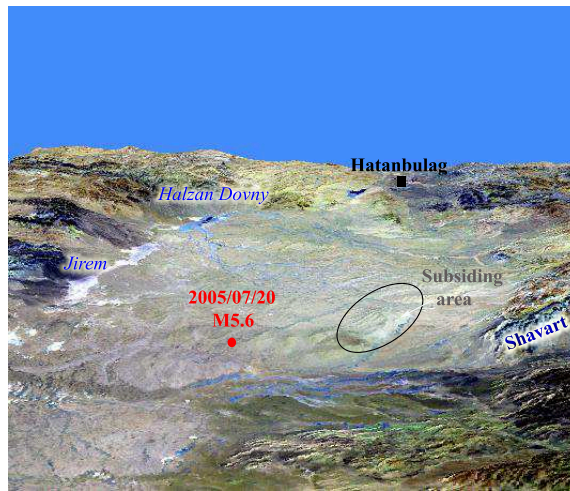

Fig. 9. 3D perspective view of the HB earthquake area from the south. SRTM DEM overlayed by LANDSAT ETM (RGB/754-wet area in blue), vertical exageration is 25, scale is M1:100000.

6. Conclusion

We analysed the co-seismic deformation of two moderate-sized earthquakes that occurred in the stable southeastern and northwestern regions of Mongolia using ASAR descending and PALSAR ascending data, respectively. Both datasets were well suited for mapping displacements in the landscapes of the corresponding study sites. The ASAR data applied for the sparsely vegetated desert region of the South East Gobi, confirmed its sensitivity to small scale displacements, revealing millimeter-scale deformations even over period of three years. The complication here is that two moderate-sized earthquakes occurred at the same place with few hours difference which can not be distinguished by the InSAR. The capability of ALOS PALSAR interferometry to produce successful results for densely vegetated areas that have been previously reported by many other authors (e.g., Aoki *et al.*, 2007) was demonstrated in the Büsiin Gol area. The main limitation of the present study was the availibility of SAR data acquired only from one direction. Therefore, in this study the InSAR data are sensitive to the location and depth but not very sensitive to the fault orientation. The two earthquakes both occurred in the upper few kilometers of the crust. The HB earthquake has a blind thrust mechanism with small left-lateral component with the geodetic moment esti-

mated to be 3.83×10^{17} (M_w 5.65). The BG earthquake has a normal motion with the geodetic moment of 5.56×10^{16} (M_w5.1). Our InSAR study of the HB earthquake reveal a minimum fault plane area of $\sim$30 km^2 which could generate a $M_w > 5.6$ earthquake. This confirms suggestion of Khilko *et al.* (1985) that this small area in the Hutag Uul craton belongs to the zone of potential seismicity of $4.5 < M < 7.0$. The revealed geometry of the fault indicates the SW-NE compressional tectonic regime of the area, which is consistent with the World Stress Map (Hiedbach *et al.*, 2008) and tectonic stresses reported by Barth and Wenzel (2010), and Xu (2001) in the adjacent region of NE China. The normal fault mechanism of the M_w5.1 BG earthquake confirm the determination of Radziminovich *et al.*, (2007) that along with strike-slip faulting the normal faults are also common in this junction zone. The InSAR derived depth supports the suggestion that earthquakes in the HBG often occure in a shallow crust.

In general, this InSAR study of earthquakes in Mongolia demonstrated that provided a sufficient amount of suitable interferometric data is available, the InSAR technique can complement sparse seismic observations of the region and may complement future seismic event relocation efforts.

References

Aki, K., Earthquake mechanism, *Tectonophysics*, **13**, pp. 423-446, 1972.

Aoki, Y., M. Furuya, and T. Kato, Coseismic deformation due to the 2007 Chuetsu-oki earthquake (M6.8), *Earth Planets.&Space*, **60**, pp. 1075-1080, 2008.

Baljinnyam, I., Bayasgalan, A., Borisov, B. A., Cisternas, A., Dem'yanovich, M.G., Ganbaatar, L., Kochetkov, V. M., Kurushin, R.A., Molnar, P., Philip, H., and Vashchilov, Yu. Ya., Ruptures of major earthquakes and active deformation in Mongolia and its surroundings, *Geological Society of America Memoir*, **181**, pp. 1-58, 1993.

Badarch, G., W. D. Cunningham, B. F. Windley, A new terrane subdivision for Mongolia: implications for the Phanerozoic crustal growth of Central Asia. *J. Asian Earth Sciences*, **21**, pp. 87-110, 2002.

Barth, A., and F. Wenzel, New constraints on the intraplate stress field of the Amurian plate deduced from light earthquake focal mechanisms, *Tectonophysics*, **482**, pp. 160-169, 2010.

Dawson, J., P. Cummins, P. Tregoning, and M. Leonard, Shallow intraplate earthquakes in Western Australia observed by Interferometric Synthetic Aperture Radar, *J. Geophys. Res.,* **113**, B11408, doi:10.1029/2008JB005807, 2008.

Delouis, B., J. Déverchère, V. Melnikova, N. Radziminovich, L. Lonke, C. Laroqque, J. F. Ritz, and San'kov, A reappraisal of the 1950 (Mw6.9) Mondy earthquake, Siberia, and its relationship to the strain pattern at the south-western end of the Baikal rift zone, *Terra Nova*, **14**, pp. 491-500, 2002.

Dugarmaa, T., A. Schlupp *et al.*, Seismic Hazard Assessment of Ulaanbaatar, capital of Mongolia. Seismic micro zoning map. *Report to the Ulaanbaatar Administration*, p.156, 2006.

Farr, T. G., P. A. Rosen, E. Caro, R. Crippen, R. Duren, S. Hensley, M. Kobrick, M. Paller, E. Rodriguez, L. Roth, D. Seal, S. Shaffer, J. Shimada, J. Umland, M. Werner, M. Oskin, D. Burbank, D. Alsdorf, The Shuttle Radar Topography Mission, *Review of Geophysics*, **45**, RG2004, 33 pp., 2007.

Feigl, K. L., A. Sergent, and D. Jacq, Estimation of an earthquake focal mechanism from a satellite radar interferogram - application to the December 4, 1992 Landers aftershock, *Geophys. Res. Lett.*, **22**, pp. 1037-1040, 1995.

Feigl, K. L., and E. Dupré, RNGCHN: a program to calculate displacement components from dislocations in an elastic half-space with applications for modeling geodetic measurements of crustal deformation, *Comput-*

ers&Geoscience, **25**, pp. 695-704, 1999.

Goldstein, R. M. and C. L. Werner. Radar interferogram filtering for geophysical applications, *Geophys. Res. Lett.*, **25(21)**, pp. 4035-4038, 1998.

Graham S. A., M. S. Hendrix, C. L. Johnson, D. Badamgarav, G. Badarch, J. Amory, M. Porter, R. Barsbold, L. E. Webb, B. R. Hacker, Sedimentary record and tectonic implications of Mesosoic rifting in southeast Mongolia, *GSA Bulletin*, **113**, No. 12, pp.1560-1579, 2001.

Hanks, T. C., and Kanamori, H., A moment magnitude scale, *Journal of Geophys. Res.*, **84(B5)**, 2348-2350, 1979.

Heidbach, O., M. Tingay, A. Barth, J. Reinecker, D. Kurfess, and B. Müller, The World Stress Map database release 2008. doi:10.1594/GFZ.WSM.Rel2008, 2008.

Jónsson, S., H. Zebker, P. Segall, and F. Amelung, Fault slip distribution of the 1999 M_w7.1 Hector Mine, California, Earthquake, estimated from Satellite Radar and GPS measurements, *Bulletin of the Seismological Society of America*, **92**, No. 4, pp. 1377-1389, 2002.

Johnson C. L., Polyphase evolution of the East Gobi basin: sedimentary and structural records of Mesozoic-Cenozoic intraplate deformation in Mongolia, *Basin Research*, **16**, pp. 79-99, 2004.

Khilko, S. D., R. A. Kurushin, V. M. Kochetkov, L. A. Misharina, V. I. Melnikova, N. A. Gilyova, S. V. Lastochkin, I. Baljinnyam, D. Monkhoo, Earthquakes and the bases of the seisminc zoning of Mongolia, Transactions, **41**, *The joint Soviet-Mongolian scientific-research geological expedition, Edited by N. S. Zaitsev et al., 222 pp, Nauka, Moscow, 1985*

Klyuchevskii, A. V., L. Selenge, V. M. Demjanovich, G. Bayar, V. I. Melnikova, N. A. Radziminovich, M. Adyaa, Kinematics and dynamics of aftershocks of the 1991 Busiingol earthquake in: *Complex geophysical and seismological investigations in Mongolia*, Edited by V. I. Dzhurik and T. Dugarmaa, 315 pp, Ulaanbaatar-Irkutsk, 2004.

Klyuchevskii, A. V., T. Dugarmaa, V. M. Demyanovich, and G. Bayart, Basic parameters and characteristics of seismicity in Mongolia. Proceedings of Conference commemorating the 50th anniversary of the 1957 Gobi-Altay earthquake, Ulaanbaatar, 2007.

Lamb, M.A., A. D. Hanson, S. A. Graham, G. Badarch, L. E. Webb, Left-lateral sense offset of upper Proterozoic to Paleozoic features across the Gobi Onon, Tost, and Zuunbayan faults in southern Mongolia and implications for other Central Asian faults, *Earth Planet. Sci.Lett.,* **173**, pp. 183-194, 1999.

Lohman, R.B., and M.Simons, Locations of selected small earthquakes in the Zagros Mountains, *Geochem. Geophys. Geosys.*, **6**, 2005.

Logachev, N. A. History and geodynamics of Baikal rift. *J. Geology and Geophysics, Russian Academy of Sciences*, **44**, 391-406, 2003 (in Russian).

Massonet, D. and K. Feigl, Radar Interferometry and its application to changes in Earth's surface. *Rev. Geophys.*, **36**, pp. 441-500, 1998.

National Atlas of the Mongolian Peoples Republic. Ulaanbaatar& Moskva, 1990.

Nissen, E., F. Yamini-Fard, M. Tatar, A. Gholamzadeh, E. Bergman, J. R. Elliott, The vertical separation of mainshock rupture and microseismicity at Qeshm island in the Zagros fold-and-thrust belt, Iran. *Earth and Planetary Science Letters*, **296**, pp. 181-194, 2010.

Okada, Y., Surface deformation due to shear and tensile faults in a half space. *Bulletin of the Seism. Soc. America*, **75**, pp. 1135-1154, 1985.

Peltzer, G., P. Rosen, F. Rogez, and K. Hudnut, Poroelastic rebound along the Landers 1992 earthquake surface rupture, *J. Geophys. Res.,* **103(B12)**, pp. 30,131-30,145, 1998.

Radziminovitch, N. A., V. I. Melnikova, M. Adyaa, D. Ankhtsetseg, L. Selenge and G. Bayar, Recent stress and strain state of the crust of the nothern Mongolia and southern Baikal regions from focal solutions, *Proceedings of the conference commemorating the 50th anniversary of the 1957 Gobi-Altay earthquake*, Ulaanbaatar, 25 July-08 August, 2007.

Scharroo, R., and P. N. A. M. Visser, Precise orbit determination and gravity field improvement for the ERS satellites, *J. Geophys. Res.,* **103**, C4, pp. 8113-8127, 1998.

Sengör, A. M. C., B. A. Natalín and V. S. Burtman, Evolution of the Altaid tectonic collage and Palaeozoic crustal growth in Eurasia. *Nature*, **364**, 1993.

Strozzi, T., U. Wegmüller, Ch. Werner and A. Wiesmann, Measurement of slow uniform surface displacement with mm/year accuracy. *IEEE Transactions on Geoscience and Remote Sensing*, 2000.

Uflyand, A. K., A. V. Ilýin and A. I. Spirkin, Basins of Baykalian type in Northern Mongolia. Translated from Vpadiny Baykalśkogo tipa Severnoy Mongolii, Byul. MOIP, otd. geol., 1969, **XLIV**, 5022, in: Internat. Geology Rev., **12**, 1980.

Webb, L. E., and C. L. Johnson, Tertiary strike-slip faulting in southeast-

ern Mongolia and implications for Asian tectonics, *Earth and Planetary Science Letters*, **241**, pp. 323-335, 2006.

Wegmüller, U., and Ch. Werner, GAMMA SAR Processor and interferometry software, *Proceedings of the 3rd ERS Symposium*, 1997.

Wright, T., B. Parsons, and E. Fieldings, Measurement of interseismic-strain accumulation across the North Anatolian Fault by satellite radar interferometry. *GRL*, **28**, pp. 2117-2120, 2001.

Xu, Z.-h, A present-day tectonic stress map for eastern Asia region. *Acta Seismol. Sin.*, **14(5)**, pp. 524-533, 2001.

Yarmolyuk, V. V., V. I Kovalenko, E. B. Sal'nikova, V. P. Kovach, A. M. Kozlovsky, A. V. Kotov, and V.I.Lebedev, Geochronology of igneous rocks and formation of the Late Paleozoic south Mongolian active margin of the Siberian continent. *Stratigraphy and Geological Correlation*, **16**, pp.162-181, 2008.

Yue,Y. and Liou, J. G., Two-stage evolution model for the Altyn Tagh fault, China. *Geology*, **27**, 227-230, 1999.

Zebker, H. A., P. A. Rosen, R. M. Goldstein, A. Gabriel, and Ch. L. Werner, On the derivation of coseismic displacement fields using differential radar interferometry: The Landers earthquake. *J. Geophys. Res.*, **99**, pp. 19617-19634, 1994.

Zonenshain L.P. and L.A. Savostin, Geodynamics of the Baikal rift zone and plate tectonics of Asia, *Tectonophysics*, **76**, pp. 1-45, 1981.

Zorin, Yu. A., E. Kh. Turutanov, and V. M. Kozhevnikov, Mantle plumes beneath the Baikal rift zone and adjacent areas: Geophysical evidence, *Doklady Earth Sciences*, **393A**, pp. 1302-1304, 2003.

Sh. Amarjargal (e-mail: amarshrgl@yahoo.com)